Efficient polynomial chaos approximations: Active, local and basis-adapted

Z. G. Ghauch[1]

(Received 7 September 2020; revised 23 May 2021)

Abstract

Metamodels provide an efficient means for the approximation of response surfaces of systems, particularly for resource-intensive experiment designs. It is oftentimes the case that interest is focused on a specific region of the parameter space. We propose an efficient recipe for the local approximation of response surfaces using Polynomial Chaos techniques. For systems embedded in high-dimensional settings, a basis-adapted spectral representation is exploited locally for dimension reduction. The proposed approach comprises an initial heuristic global solution for parameter space exploration using an approximate global Polynomial Chaos metamodel, followed by a local design being refined through an active learning scheme. The problem of turbulent flow around a symmetric airfoil is considered. Statistical estimators based on the local, active, basis-adapted approach show less bias and faster convergence as compared to the estimators from a global solution.

DOI:10.21914/anziamj.v62i0.15833, Published 2021-06-08, as part of the Proceedings of the 19th Biennial Computational Techniques and Applications Conference. ISSN 1445-8810. (Print two pages per sheet of paper.)

Contents

1 Introduction

In a plethora of domains, such as uncertainty quantification and optimization, metamodels have proved their worth for efficiently approximating responses of systems. In particular, metamodels play a central role for problems that involve expensive-to-evaluate designs. To approximate the response surface of such resource-intensive models, a metamodel training algorithm that minimizes the size of the experiment without loss of accuracy is essential.

Multiple studies examined the experiment design problem for metamodel response surface approximation [10, 3, 1]. An adaptive experiment design approach for local metamodel approximation over a region of interest of the parameter space using a weighted integrated mean squared error was proposed by Picheny et al. [10]. Another study used optimal experiment designs through active learning for reliability purposes [1]. A detailed review

of metamodels within the scope of the design of experiment settings is outside the scope of this work.

In some practical applications, interest is focused on a specific region of the parameter space. As such, local, variance-optimal experiment designs, could be exploited to satisfy, ideally, a suite of factors [2], including minimizing the size of the experiment design, providing error estimates at every design phase, accommodating increasingly complex designs in a sequential scheme, maximizing the accuracy of the fit, and providing a measure of lack of fit. Moreover, one challenge that still stands in the way of conventional metamodels is the so-called curse of dimensionality some metamodels face in high-dimensional parameter spaces.

2 Formulation

2.1 Overview

Let $\mathcal{G}$ denote the parameter space, and $\mathcal{L} \subset \mathcal{G}$ the region of interest. A global heuristic solution is initially obtained based on a space-filling design of $\mathcal{G}$, from which a region of interest $\mathcal{L}$ can be obtained based, for example, on a maximization of some objective function centered on information gain or local uncertainty. The global heuristic solution involves essentially a low-order Polynomial Chaos (PC) metamodel over $\mathcal{G}$ from which a region of interest $\mathcal{L}$ is identified and a local metamodel is built over $\mathcal{L}$. Once we identify a local region $\mathcal{L}$ in the parameter space $\mathcal{G}$ based on an information gain criterion evaluated from the heuristic solution from the global PC metamodel, efforts are focused on the experiment design at the local metamodel. Specifically, an active sampling scheme is leveraged at the local metamodel level to sequentially refine the local design. At the local metamodel level over $\mathcal{L}$, a basis-adapted PC formulation is proposed as a dimension reduction scheme for problems embedded in high-dimensional settings. The local PC metamodel over $\mathcal{L}$ is adaptively refined until some predefined convergence criteria are met.

2.2 Global/local approximations

Following the global/local methodology adopted herein, consider a global metamodel and a corresponding local metamodel as approximations to the true response of a given system. Consider a space-filling design, denoted by $\mathcal{H}^{\mathcal{G}}$, tailored for building the global metamodel over the parameter space and consisting of $N_{\mathcal{G}}$ space-filling design samples, with input $\mathbf{X}^{\mathcal{G}}$ and corresponding output $Y^{\mathcal{G}}$, that is $\mathcal{H}^{\mathcal{G}} : \mathbf{X}^{\mathcal{G}} = (x_1, \dots, x_{N_{\mathcal{G}}})$, $Y^{\mathcal{G}}(\mathbf{X}^{\mathcal{G}}) = (y_1, \dots, y_{N_{\mathcal{G}}})$, $i = 1, \dots, N_{\mathcal{G}}$, $x_i \in \mathcal{G}$. Similarly, let $\mathcal{H}^{\mathcal{L}}$ denote a space-filling design for the local metamodel consisting of $N_{\mathcal{L}}$ design points build over the subregion $\mathcal{L} \subset \mathcal{G}$, that is $\mathcal{H}^{\mathcal{L}} : \mathbf{X}^{\mathcal{L}} = (x_1, \dots, x_{N_{\mathcal{L}}})$, $Y^{\mathcal{L}}(\mathbf{X}^{\mathcal{L}}) = (y_1, \dots, y_{N_{\mathcal{L}}})$, whereby $i = 1, \dots, N_{\mathcal{L}}$, $x_i \in \mathcal{L}$. The global PC metamodel is trained with respect to the space-filling design in the global domain $\mathcal{H}^{\mathcal{G}}$, while the local PC metamodel is built using the space-filling design $\mathcal{H}^{\mathcal{L}}$ over $\mathcal{L}$. We adopted the Maximin algorithm [7] as a space-filling design for the training of both the local and global metamodels.

2.3 Active sampling

In the proposed active sampling formulation, adaptive samples are appended to the local design set $\mathcal{H}^{\mathcal{L}}$. The local space-filling design set is sampled optimally in a sequential scheme. At each iteration, the next design sample is selected based on a maximization of the functional representation of the information gain evaluated at the current step, following $\mathcal{H}^{\mathcal{L}}_{i+1} = \mathcal{H}^{\mathcal{L}}_i \cup x^*_i$, $i = 1, \dots, N_{\mathcal{L}}$, $x^*_i \in \mathcal{L}$. We aim at finding an optimal choice of $\mathbf{X}^{\mathcal{L}}$ such that the ensuing metamodel best approximates the response surface locally with the fewest design samples.

2.4 Basis-adapted polynomial chaos

Consider a probability space $(\Omega, \mathcal{F}, P)$ consisting of a sample space Ω, a σ-algebra $\mathcal{F}$ on Ω, and a corresponding probability measure P on $(\Omega, \mathcal{F})$. For a Quantity of Interest (QoI) q, defined as a function of d-dimensional

random input parameters $\xi \in \mathbb{R}^d$ on Ω, for some forward operator F, we have $q = F(\xi)$. Under the finite variance assumption, that is $q \in L^2(\Omega, \mathcal{F}, P)$, the random variable $q : \Omega \to \mathbb{R}$ admits a spectral representation following a PC expansion [4]

$$q(\xi) = \sum_{\alpha} q_\alpha \Psi_\alpha(\xi), \tag{1}$$

where $\boldsymbol{\alpha}$ represents a multi-index that associates for each variable $\{\xi_i\}_{i=1}^d$ a degree of the multivariate polynomial $\Psi_{\boldsymbol{\alpha}}$ with corresponding coefficients $q_{\boldsymbol{\alpha}}$. The latter can be expressed in terms of the corresponding univariate polynomials. Let $\mathbf{c}$ denote the vector of coefficients that we are solving for and $\mathbf{u}$ the corresponding output vector. Consider M realizations of the random system inputs, and a truncated form of equation (1) with only K terms. The Vandermonde design matrix $\boldsymbol{\Psi}$ can be defined as $\boldsymbol{\Psi} = [\Psi_{ij}]$, $\Psi_{ij} = \Psi_{\boldsymbol{\alpha}^{(j)}}(\boldsymbol{\xi}^{(i)})$, $i \in [1, M]$, $j \in [1, K]$. We solve the l_2 minimization problem of the form

$$\mathbf{c}^* = \arg\min_{\mathbf{c}} \|\boldsymbol{\Psi}\mathbf{c} - \mathbf{u}\|_2 . \tag{2}$$

It is evident at this point that as the number of random inputs increase, the size of the vector of coefficients $\mathbf{c}$ increases beyond what practical numerical recipes can efficiently solve. To address this issue, basis adaption techniques have been developed [12], and applied successfully in forward [6], inverse [13, 5], and optimization under uncertainty problems [11]. Tipireddy and Ghanem [12] review in detail the theoretical background behind basis-adapted PC.

2.5 Expected feasibility function

Let $\text{EFF}^{\mathcal{G}}$ define the Expected Feasibility Function evaluated from the global metamodel over the parameter space $\mathcal{G}$, and $\text{EFF}_i^{\mathcal{L}}$ the corresponding Expected Feasibility Function evaluated at the local metamodel over a region of interest $\mathcal{L}$ at the ith iteration of the active learning scheme. Let $\mathbb{1}_{\mathcal{L}}[x]$, $x \in \mathcal{G}$, denote the indicator function corresponding to target region $\mathcal{L}$. Given the variance $\tilde{\sigma}^2(x)$, $x \in \mathcal{G}$, a measure of local uncertainty along the target

region $\mathcal{L}$ is [2]

$$\text{EFF}_i^{\mathcal{L}} := \int_{\mathcal{L}} \tilde{\sigma}_i^2(x)\,dx = \int_{\mathcal{G}} \tilde{\sigma}_i^2(x)\mathbb{1}_{\mathcal{L}}[x]\,dx\,, \quad i = 1,\ldots,N_{\mathcal{L}}\,. \tag{3}$$

While $\text{EFF}^{\mathcal{G}}$ is defined over $\mathcal{G}$ based on design $\mathcal{H}^{\mathcal{G}}$, $\text{EFF}_i^{\mathcal{L}}$ is evaluated locally over $\mathcal{L}$ based on design samples $\mathcal{H}^{\mathcal{L}}$. At the ith iteration of the active learning scheme, we have

$$x_i^* = \underset{x\in\mathcal{L}}{\text{argmax}}\, \tilde{\sigma}_i^2(x)\,, \quad i = 1,\ldots,N_{\mathcal{L}}\,. \tag{4}$$

We further propose a local averaging metric to improve the performance of the active learning scheme on nonlinear response surfaces by applying Kernel Smoothing (i.e. Nearest Neighbor Smoother).

In a basic sense, PC metamodels do not provide a local measure of uncertainty. To that end, a Bootstrap resampling scheme was successfully adopted. The bootstrap resampling scheme was leveraged to obtain a measure of local variability as determined by the uncertainty in the PC coefficients due to the limited size of the experiment design [8]. For B bootstrap samples, equation (2) was solved for each sample $b = 1,\ldots,B$.

2.6 Error and convergence

For convergence assessment, two different error metrics are examined: the well-known Mean Squared Error (MSE), and another metric based on the absolute relative error. For the latter, the convergence criteria is based on an expression of the relative error of a statistical estimator following

$$\varepsilon_j = \frac{\mathbb{E}_{\mathcal{L}}[|\hat{q}_j^{\mathcal{L}}(\xi_{N_{MC}}^{\mathcal{L}}) - y(\xi_{N_{MC}}^{\mathcal{L}})|^2]}{\mathbb{E}_{\mathcal{L}}[|\hat{q}_j^{\mathcal{L}}(\xi_{N_{MC}}^{\mathcal{L}})|^2]}\,, \quad j = 1,\ldots,N_{\mathcal{L}}\,, \tag{5}$$

where $\xi_{N_{MC}}^{\mathcal{L}}$ denotes the Monte Carlo samples within the region of interest $\mathcal{L}$, y the corresponding observations, and $\hat{q}_j^{\mathcal{L}}$ the corresponding predictions from

the local PC metamodel at the jth active learning step. For consistency, for all the cases examined, even that of a global metamodel, we compute the error metrics with respect to $\mathcal{L}$.

3 Numerical applications and results

3.1 Quadratic polynomial

Consider a d-dimensional, second-order polynomial function $f : \mathbb{R}^d \to \mathbb{R}$ of the form

$$f(\boldsymbol{\xi}) = \beta_0 + \boldsymbol{\beta}_1^T \boldsymbol{\xi} + \boldsymbol{\xi}^T \boldsymbol{\beta}_2 \boldsymbol{\xi}, \tag{6}$$

where $\{\xi\}_{i=1}^d$ are sampled from a Uniform distribution following $\{\xi\}_{i=1}^d \sim \mathcal{U}(-2, 2)$, $\boldsymbol{\beta}_1 \sim \mathbb{R}^{d\times 1}$ and $\boldsymbol{\beta}_2 \sim \mathbb{R}^{d\times d}$ represent a vector and a matrix of coefficients, respectively. Consider a two-dimensional representation of equation (6) with coefficients $\beta_0 = 0.803$, $\boldsymbol{\beta}_1 = [0.527; 0.119]$, and $\boldsymbol{\beta}_2 = [0.296, 0.301; 0.031, 0.336]$. Let $q_\Gamma(\boldsymbol{\xi})$ denote a given QoI defined at the corner of the parameter space, that is $(2, 2)$. For this validation problem, a total of $B = 100$ bootstrap samples were used.

3.2 Turbulent flow over airfoil

Going beyond the mathematical function of equation (6), consider the problem of turbulent flow over a symmetric airfoil. The model geometry corresponds to a NACA 0012 airfoil adapted from NASA [14]. The physics of the problem involves turbulent, incompressible, subsonic, steady flow over the symmetric airfoil. The computational fluid dynamics solver from the OpenFOAM [9] suite was used. The airfoil boundary consists of an inlet on the left boundary, wind tunnel walls at the top and bottom boundaries, and outlet along the right boundary [14]. Let p, ν and $\mathbf{u}$ denote the pressure, kinematic viscosity, and velocity, respectively. For an incompressible flow with spatially-uniform viscosity, the Navier–Stokes equations take the form

$$\frac{\partial \mathbf{u}}{\partial t} + (\mathbf{u} \cdot \nabla)\mathbf{u} = -\nabla p + \nu \nabla^2 \mathbf{u}, \tag{7}$$

$$\nabla \cdot \mathbf{u} = 0\,. \tag{8}$$

The QoI in this airfoil problem is the dimensionless lift coefficient C_L. Once the velocity field $\mathbf{u}$ is computed, the lift coefficient QoI C_L can be evaluated based on the lift force, the wing area, fluid density and velocity. The random input parameters of the 6D turbulent flow over airfoil problem consist of: angle of attack $\alpha(^\circ) \sim \mathcal{U}(6.4, 9.6)$, density $\rho \sim \mathcal{U}(0.95, 1.42)$ (kg/m^3), viscosity $\nu \sim \mathcal{U}(1.2, 1.8) \times 10^{-5}$ (m^2/s), kinematic viscosity $\nu_t \sim \mathcal{U}(0.11, 0.17)$ (m^2/s), far-field velocity $U_x \sim \mathcal{U}(8.3, 9.7)$ (m/s) and thickness ratio $t/c \sim \mathcal{U}(0.11, 0.13)$.

3.3 Results

Convergence results for the two-dimensional quadratic polynomial are presented in Figures 1 and 2. Figure 1(a) shows the true response function of the quadratic polynomial, along with the corresponding space-filling design used for training of the low-order (i.e., first order) global PC metamodel approximation. Figure 1(b) shows the $\text{EFF}^{\mathcal{G}}$ function across the domain at the end of the first-order global PC approximation phase before any adaptive sampling is conducted. In this problem, the region of interest $\mathcal{L}$ for the local PC metamodel was selected in the neighborhood of the point that maximizes the $\text{EFF}^{\mathcal{G}}$ function from the initial global metamodel approximation, which corresponds to the corner of the parameter space $\mathcal{G}$, that is $(\xi_1, \xi_2) = (2, 2)$, as shown in Figure 1(c).

Figures 1(c–j) show the $\text{EFF}^{\mathcal{L}}$ function and the corresponding local, PC-based response surface approximation $\widehat{f}$ at four steps of the local metamodel refinement following the active learning scheme.

Figure 2 shows the corresponding convergence results for the two-dimensional quadratic polynomial during the local adaptive sampling phase. Figure 2(a) shows the sampling scheme of the proposed methodology, including the space-filling design used to train the global PC metamodel approximation $\mathcal{H}^{\mathcal{G}}$, the Monte Carlo samples $\boldsymbol{\xi}^{\mathcal{L}}_{\text{MC}}$ in the region of interest $\mathcal{L}$, and the adaptive samples $\mathcal{H}^{\mathcal{L}}$ at the end of the refinement-via-active-learning phase over the

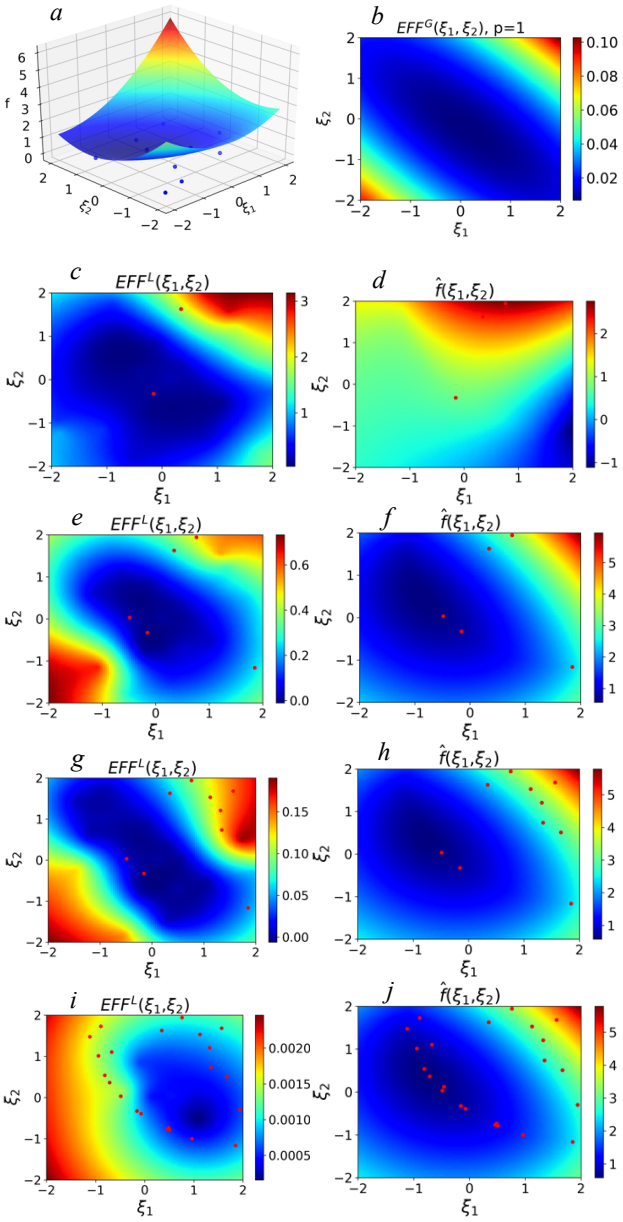

Figure 1: Local response function approximation for the two-dimensional quadratic polynomial.

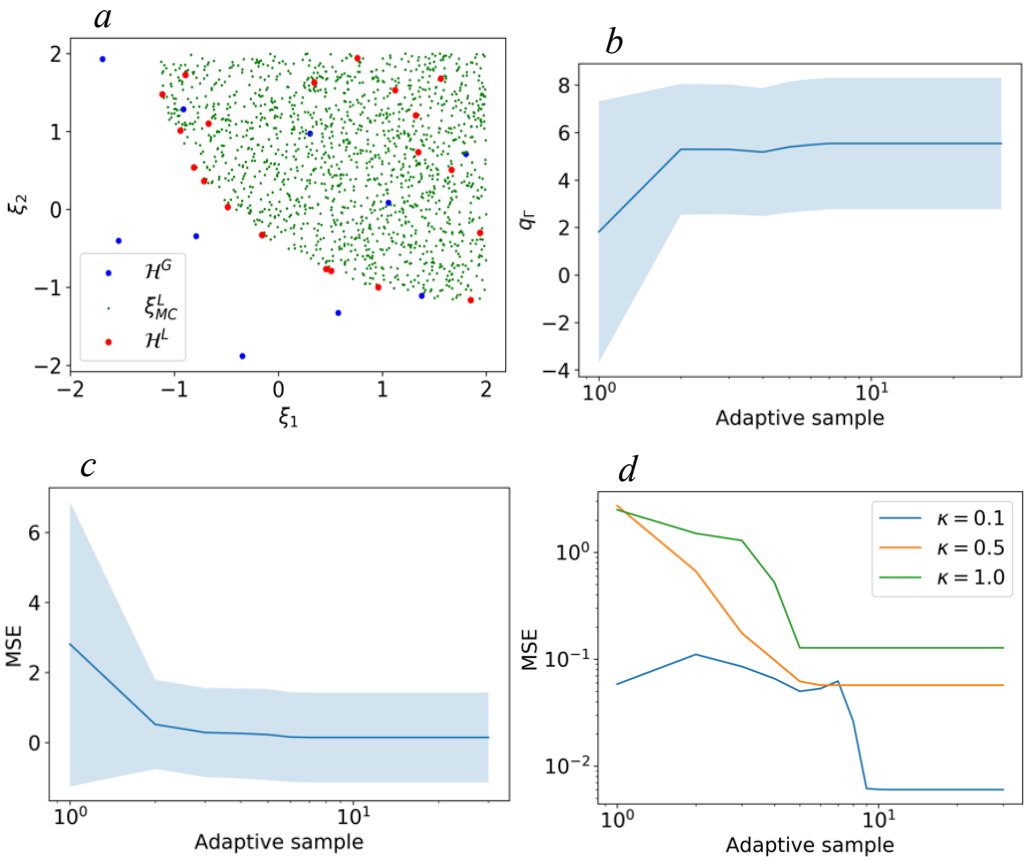

Figure 2: Convergence for the two-dimensional quadratic polynomial.

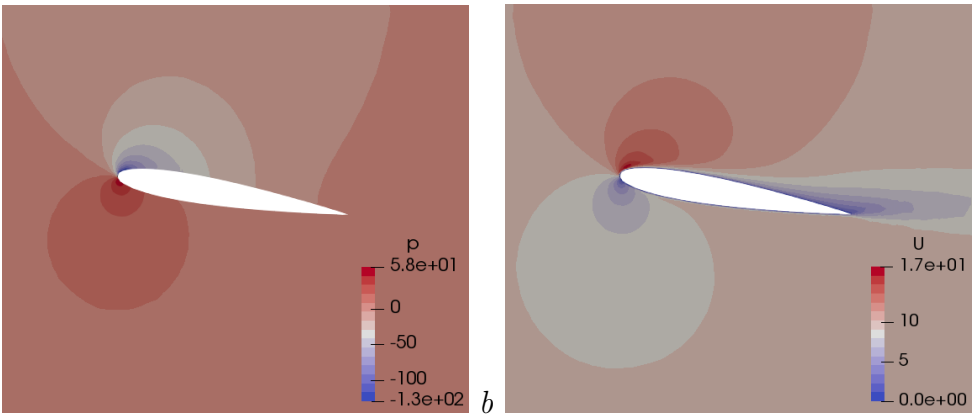

Figure 3: Contours of (a) pressure $\mathfrak{p}$ and (b) velocity $\mathfrak{u}$ fields around the airfoil.

local region $\mathcal{L}$. Figure 2(b) shows the convergence of the QoI $\mathfrak{q}_\Gamma$ defined in the corner of the parameter space near $(\xi_1, \xi_2) = (2, 2)$. Figure 2(c) shows the convergence in terms of MSE. Figure 2(d) shows the convergence in terms MSE for different sizes κ of the region of interest $\mathcal{L}$. It is observed that a smaller region of interest κ over which the local metamodel is trained results in a lower level of error across all the active learning iterations.

Preliminary results for the problem of turbulent flow over the airfoil are presented in Figure 3, which shows the contour of the pressure field $\mathfrak{p}$ and velocity $\mathfrak{u}$ in the vicinity of the airfoil model at the final numerical step for a random realization. Figure 4(a) shows the probability density function of the QoI C_L at the end of the active learning phase for the global PC metamodel ($\kappa = 1.0$) and the local PC metamodel ($\kappa = 0.2$). A benchmark solution corresponding to 2000 Monte Carlo samples in the region of interest $\mathcal{L}$ where the local metamodel was trained is also shown. It is observed that at the end of the active training window investigated herein, the local PC metamodel captures the true probabilistic solution (as approximated by the Monte Carlo samples) better than the global PC metamodel. The statistical estimator from the global PC metamodel shows more bias at the end of the

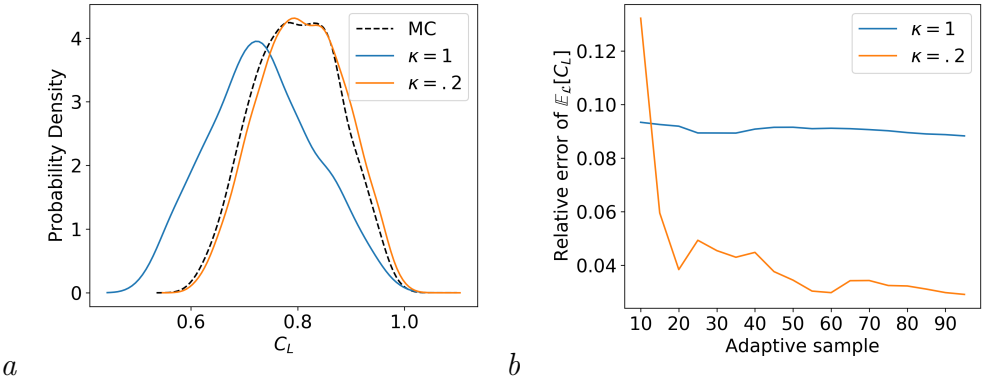

Figure 4: Convergence for the turbulent flow over airfoil problem (a) probability density function of QoI, (b) relative error in the active sampling phase.

adaptive training window than the corresponding estimator from the local PC metamodel. Figure 4(b) shows the relative error of the statistical estimator for C_L throughout the active learning phase. The estimator for C_L based on the local PC metamodel ($\kappa = 0.2$) consistently shows better performance than the estimator based on a global PC metamodel ($\kappa = 1.0$).

4 Findings and conclusions

We addressed the problem of performing efficient local response surface approximations with state-of-the-art PC techniques. Specifically, we employed a basis adaptation scheme for dimension reduction at the local PC metamodel level. Our proposed methodology is centered on a coupled global/local PC metamodel scheme, followed by an active sampling of the local metamodel over a target region of interest. We observed that the statistical estimators obtained from a globally accurate solution show more bias throughout the adaptive sampling phase than the corresponding estimator from a local metamodel.

References

[1] B. J. Bichon, M. S. Eldred, L. P. Swiler, S. Mahadevan, and J. M. McFarland. "Efficient global reliability analysis for nonlinear implicit performance functions". In: *AIAA J.* 46.10 (2008), pp. 2459–2468. DOI: 10.2514/1.34321 (cit. on p. C17).

[2] G. E. P. Box and N. R. Draper. *Empirical Model-Building and Response Surfaces*. Wiley, 1987 (cit. on pp. C18, C21).

[3] V. Dubourg, B. Sudret, and F. Deheeger. "Metamodel-based importance sampling for structural reliability analysis". In: *Prob. Eng. Mech.* 33 (2013), pp. 47–57. DOI: 10.1016/j.probengmech.2013.02.002 (cit. on p. C17).

[4] R. G. Ghanem and P. D. Spanos. *Stochastic finite element: A spectral approach*. Dover, 1991. DOI: 10.1007/978-1-4612-3094-6 (cit. on p. C20).

[5] Z. G. Ghauch. "Leveraging adapted polynomial chaos metamodels for real-time Bayesian updating". In: *J. Verif. Valid. Uncert.* 4.4 (2020), p. 041003. DOI: 10.1115/1.4045693 (cit. on p. C20).

[6] Z. G. Ghauch, V. Aitharaju, W. R. Rodgers, P. Pasupuleti, A. Dereims, and R. G. Ghanem. "Integrated stochastic analysis of fiber composites manufacturing using adapted polynomial chaos expansions". In: *Compos. Part A: Appl. Sci.* 118 (2019), pp. 179–193. DOI: 10.1016/j.compositesa.2018.12.029 (cit. on p. C20).

[7] M. E. Johnson, L. M. Moore, and D. Ylvisaker. "Minimax and maximin distance designs". In: *J. Stat. Plan. Infer.* 26.2 (1990), pp. 131–148. DOI: 10.1016/0378-3758(90)90122-B (cit. on p. C19).

[8] A. Notin, N. Gayton, J. L. Dulong, M. Lemaire, P. Villon, and H. Jaffal. "RPCM: A strategy to perform reliability analysis using polynomial chaos and resampling". In: *Euro. J. Comput. Mech.* 19.8 (2010), pp. 795–830. DOI: 10.3166/ejcm.19.795-830 (cit. on p. C21).

[9] OpenCFD. *OpenFOAM User's Guide*. 2019. URL: https://www.openfoam.com/documentation/user-guide (cit. on p. C22).

[10] V. Picheny, D. Ginsbourger, O. Roustant, R. T Haftka, and N.-H. Kim. "Adaptive designs of experiments for accurate approximation of target regions". In: *J. Mech. Design.* 132.7 (2010), p. 071008. DOI: 10.1115/1.4001873 (cit. on p. C17).

[11] C. Thimmisetty, P. Tsilifis, and R. Ghanem. "Homogeneous chaos basis adaptation for design optimization under uncertainty: Application to the oil well placement problem". In: *AI EDAM* 31.3 (2017), pp. 265–276. DOI: 10.1017/S0890060417000166 (cit. on p. C20).

[12] R. Tipireddy and R. Ghanem. "Basis adaptation in homogeneous chaos spaces". In: *J. Comput. Phys.* 259 (2014), pp. 304–317. DOI: 10.1016/j.jcp.2013.12.009 (cit. on p. C20).

[13] P. Tsilifis and R. G. Ghanem. "Reduced Wiener chaos representation of random fields via basis adaptation and projection". In: *J. Comput. Phys.* 341 (2017), pp. 102–120. DOI: 10.1016/j.jcp.2017.04.009 (cit. on p. C20).

[14] *Turbulence Modeling Resource*. NASA Langley Research Center. Washington, DC (2018). URL: http://turbmodels.larc.nasa.gov/ (cit. on p. C22).

Author address

1. **Z. G. Ghauch**, School of Engineering, University of California Berkeley, Berkeley 94720, United States.
mailto:ghauch@alumni.usc.edu
orcid:0000-0002-1961-7655